Exp Fluids (2016) 57:95
DOI 10.1007/s00348-016-2183-z

RESEARCH ARTICLE

Color gradient background-oriented schlieren imaging

Frank Austin Mier[1] · **Michael J. Hargather**[1]

Received: 16 January 2016 / Revised: 2 May 2016 / Accepted: 3 May 2016

Abstract Background-oriented schlieren is a method of visualizing refractive disturbances by comparing digital images with and without a refractive disturbance distorting a background pattern. Traditionally, backgrounds consist of random distributions of high-contrast color transitions or speckle patterns. To image a refractive disturbance, a digital image correlation algorithm is used to identify the location and magnitude of apparent pixel shifts in the background pattern between the two images. Here, a novel method of using color gradient backgrounds is explored as an alternative that eliminates the need to perform a complex image correlation between the digital images. A simple image subtraction can be used instead to identify the location, magnitude, and direction of the image distortions. Gradient backgrounds are demonstrated to provide quantitative data only limited by the camera's pixel resolution, whereas speckle backgrounds limit resolution to the size of the random pattern features and image correlation window size. Quantitative measurement of density in a thermal boundary layer is presented. Two-dimensional gradient backgrounds using multiple colors are demonstrated to allow measurement of two-dimensional refractions. A computer screen is used as the background, which allows for rapid modification of the gradient to tune sensitivity for a particular application.

✉ Michael J. Hargather
mjh@nmt.edu

[1] New Mexico Tech, 801 Leroy Pl., Socorro, NM 87801, USA

1 Introduction

The background-oriented schlieren (BOS) technique has become one of the most widely used refractive flow visualization techniques of the digital age. The technique visualizes a refractive disturbance via its apparent background distortion, requiring digital processing of the images to reveal the refractive disturbance (Raffel 2015). The computer processing required to produce the image differentiates the BOS technique from traditional schlieren and shadowgraph techniques which directly image refractive disturbances using optical elements, knife edges, and screens (Settles 2001).

The broad topic of BOS imaging and analysis has recently been reviewed by Raffel (2015). The technique was first introduced almost simultaneously by Dalziel et al. (2000) as "synthetic schlieren" and Raffel et al. (2000) as a "background-oriented optical density gradient technique." Current uses of the technique include qualitative and quantitative imaging for wind tunnels (Ota et al. 2015; Venkatakrishnan and Suriyanarayanan 2009; Venkatakrishnan and Meier 2004), nozzles (Tan et al. 2015), microjets (Kumar et al. 2011), full-scale helicopters in flight (Bauknecht et al. 2015), and explosions at laboratory- (Venkatakrishnan et al. 2013) and full-scales (Hargather 2013), among many other applications.

The BOS technique yields images of refractive fields by comparing digital images of a background with and without a refractive disturbance. The two digital images are processed using a cross-correlation algorithm to obtain a measure of the "shift" in the background pixels between the images with and without the refractive disturbance. The magnitude of this pixel shift can be quantitatively related to the imaged refractive index field, yielding the density

Published online: 17 May 2016

field for simple objects and known setup geometry (Elsinga et al. 2004; Hargather and Settles 2012). Typically a random "speckle" pattern is used as the background (Raffel 2015), although many researchers have demonstrated the use of natural backgrounds (Bauknecht et al. 2015; Richard and Raffel 2001; Hargather and Settles 2010). As long as the background has sufficient uniqueness, the ability to obtain quantitative refractive field information is solely dependent on the ability to perform a cross-correlation on the images to obtain the apparent pixel motion.

Several researchers have attempted to enhance BOS accuracy and sensitivity through more accurate cross-correlation routines. Their approaches have developed enhanced backgrounds using speckle patterns with wavelet noise (Atcheson et al. 2009) or colors (Leopold 2009) to yield more unique correlations. These approaches, however, still require the cross-correlation, which can be a time-consuming computational process and results in an inherent averaging of the pixel shift measurement over some correlation window area. While modern computers can perform cross-correlation tasks in reasonable time frames, the number of individual calculations needed for a cross-correlation is still large and scales with search window size.

Here, a new approach is presented wherein a gradient background is used to allow an image subtraction analysis to be performed to yield a quantitative BOS image. This approach provides pixel-level resolution and a simple processing algorithm which could be easily automated to allow near-real-time BOS imaging. The sensitivity, or measurement range, of the BOS system can be tuned by varying the gradient pattern size, which is done easily here with the use of a computer monitor as the background.

2 Quantitative BOS procedures

The BOS system consists of a camera, background, and refractive object of interest. These components are arranged linearly along an axis representing the center of the camera's field of view, as shown in Fig. 1. The distance between the camera and refractive object (t) is less than the distance from the camera to the background (L), and the distance to the refractive object is typically greater than $0.75L$ for good photography and maintaining both the background and refractive object in acceptable focus (Hargather and Settles 2012). Decreasing this ratio toward $0.5L$, however, provides greater apparent background distortion and more sensitivity, but becomes more difficult to keep the object in sharp focus with a limited depth of focus camera lens. Sensitivity is analogous to the smallest angle of refraction (ε) that can be resolved. This angle is defined for a position in the refractive object from the camera axis (r) and relates to the apparent distortion of the background (e or "pixel shift"). The angle between the light ray passing through point r and the camera axis is denoted as θ.

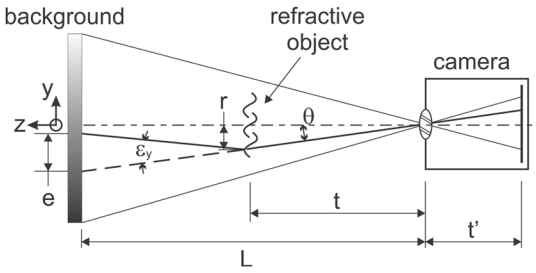

Fig. 1 Geometry of BOS system

The pixel shift on the background plane (e) can be calculated from the system geometry:

$$e = (L - t)[\tan(\theta) - \tan(\theta - \varepsilon)] \tag{1}$$

The angles ε and θ are small, thus the small angle approximation for tangent can be used ($\tan\varepsilon \approx \varepsilon$), simplifying to:

$$e = (L - t)\varepsilon \tag{2}$$

Light traveling in the z-direction is refracted in the y-direction through an angle ε_y due to a refractive index (n) gradient in the y-direction. For a two-dimensional schliere of extent Z along the z-direction the refraction angle is given by:

$$\varepsilon_y = \frac{1}{n}\int \frac{\partial n}{\partial y}\partial z = \frac{Z}{n_\infty}\frac{\partial n}{\partial y} \tag{3}$$

with the baseline index of refraction in the media n_∞. The index of refraction gradient is measured along an axis orthogonal to the camera axis and can be expressed in multiple directions, i.e., a vertically varying gradient ($\partial n/\partial x$) or a horizontally varying gradient ($\partial n/\partial y$), with respect to the Eulerian coordinates of the laboratory setting.

For a gas, the Gladstone–Dale relation correlates density (ρ) to the refractive index:

$$n = k\rho + 1 \tag{4}$$

where k is the Gladstone–Dale constant for a material ($k = 2.23 \times 10^{-4}$ m^3/kg for air).

Through these relationships, accurate measurements of light refraction or BOS pixel shifts can thus be correlated to index of refraction and density profiles for an imaged area. Other properties including pressure and temperature can be calculated using appropriate thermodynamic relationships including the ideal gas law.

Size and location of flow or other refractive features in the imaging plane of the test area can be measured from the BOS images, with a calibration of pixel-to-length scales using fiducials and accounting for the diverging light geometry as appropriate. Parameters associated with the

z-axis, such as the extent of a schliere Z, must be measured or assumed as the test images will only represent the two spatial axes x and y.

2.1 Calibration lens

A lens will predictably refract light due to the variation in glass thickness and thus refractive index gradient across the object. A lens thus provides a means to calibrate BOS or other refractive imaging systems (Hargather and Settles 2012). The angle at which light is refracted through a lens (ε) is dependent on the focal length (f) of the lens and the radial position through the lens (r) that the light passes:

$$\frac{r}{f} = \tan\varepsilon \approx \varepsilon \tag{5}$$

A 25.4-mm-diameter lens with a 4 m focal length (CVI PLCX-25.4-2060.0-C) was used here as the calibration object with known refractions. The focal length of the lens is chosen for the magnitude of the refraction angles to be measured and can be chosen as desired based on the geometry and sensitivity of the system being studied.

2.2 Laminar free convection flat plate boundary layer

To validate the quantitative BOS density measurement, a vertically oriented heated flat plate thermal boundary layer was chosen as a simple flow field to analyze (Hargather and Settles 2012). The free convection boundary layer on the heated surface was analytically solved for the density field near the plate by Ostrach (Ostrach 1952). The solution is in terms of a similarity length parameter (η) defined by the distance from the bottom of the flat plate (x) and horizontally from the surface of the plate (y):

$$\eta = \left(\frac{Gr_x}{4}\right)^{\frac{1}{4}} \frac{y}{x} \tag{6}$$

where the Grashof number (Gr_x) is defined as:

$$Gr_x = \frac{g\beta(T_s - T_\infty)x^3}{\nu^2} \tag{7}$$

The value for gravitational acceleration (g) is 9.807 m/s^2 and the coefficient of thermal expansion for air (β) is 0.003 K^{-1}. The plate surface (T_s) and ambient (T_∞) temperatures are measured for each test, and the kinematic viscosity for air (ν) is found from the ambient temperature.

Upon calculation of the length parameter and Grashof number, Ostrach's figures can be used to find non-dimensional temperature ($H(\eta)$) values and thus determine the temperature (T) distribution across the thermal boundary layer (Ostrach 1952):

$$H(\eta) = \frac{T - T_\infty}{T_s - T_\infty} \tag{8}$$

Here a 152 mm wide × 152 mm tall × 6 mm thick aluminum flat plate was used. The plate was heated by a resistive heating element which was affixed to the back of the plate and powered by a variable AC power supply. The plate surface temperature was measured with a K-type thermocouple affixed to the front of the plate which was removed immediately prior to imaging. Ambient temperature was measured by a K-type thermocouple suspended in the ambient air away from the plate. Imaging occurred once the surface temperature reached steady state for a period of 5 min. Care was taken to align the face of the flat plate parallel to the camera's centerline axis.

3 Gradient backgrounds

Traditional BOS imaging uses speckled backgrounds which consist of randomly distributed black-and-white regions as seen in Fig. 2. The high contrast between the speckles provides distinct features for detecting pixel shifts between flow and no-flow images, and the random distribution eliminates any bias which may occur if the contrasts were manually arranged or repeating. Conversely, a gradient background contains only smooth variations in pixel intensities.

When considering the single pixel interface between two speckles and two adjacent pixels on a gradient, the speckle background provides an easy identification of the refractive pixel shift when a light-dark boundary is crossed. When a shift occurs inside a single speckle, however, there is no direct method by which it can be detected. Modern BOS approaches have addressed this issue by developing and incorporating a range of sub-pixel resolution approaches, including optical flow algorithms (Atcheson et al. 2009), or commercial particle image

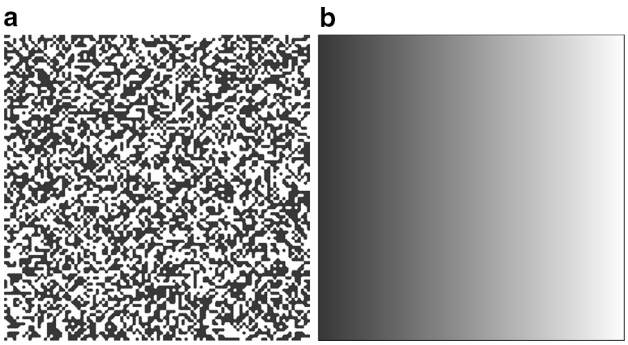

Fig. 2 Examples of **a** traditional BOS background with a randomly generated speckle pattern and **b** novel grayscale gradient background used here

velocimetry (PIV) or digital image correlation (DIC) algorithms. Many of these approaches fit curves to the pixel intensity field for the background and flow images, then correlate the curve shapes to produce deformation measurements. The ultimate resolution that can be achieved is still related to the speckle size and the unique features present in the speckle patterns.

Gradient backgrounds provide a simple means to calculate the magnitude of a pixel shift via an image subtraction between flow and no-flow images. The magnitude of the difference in intensity values at each pixel (ΔI) represents the pixel shift along the known background gradient pattern. The sign of the difference in the image subtraction determines the direction of the shift. The use of a gradient background thus allows for full quantification of the image shifts through the use of a simple image subtraction. This pixel-by-pixel subtraction yields resolution of pixel shifts equal to the pixel resolution of the image. In practice, the minimum detectable pixel shift is dependent on each pixel having a unique intensity value and thus is related to the bit-depth of the recorded images. The gradient background could be fit with a curve for sub-pixel resolution, but this is not explored here as the focus is on limiting the required computational processing.

While image subtraction has been performed in traditional BOS analysis and backgrounds, the resulting difference only highlights where shifts occurred and not the magnitude of the shift (Hargather 2013; Hargather and Settles 2010). There is no true way of quantifying the magnitude of image shifts with a speckled background and image subtraction because no inferences can be made about the area surrounding individual pixels as the distribution is inherently random. With a speckle background, quantification of shift magnitude and direction can only be achieved through image correlation.

The gradient backgrounds used here are created with linearly varying values along one of the Cartesian coordinate axes, as shown in Fig. 3a. In grayscale gradient tests, the background varies between black (0) and white (1) pixel values along a single axis. All tests presented use linearly varying backgrounds to simplify the analysis: with a linear gradient, intensity change directly correlates to pixel shift. Measuring the change in intensity (ΔI) is the same as measuring a pixel shift (e):

$$e = \Delta I \left(\frac{\text{Pixel}}{\text{Intensity}} \right) \left(\frac{\text{Length}}{\text{Pixels}} \right) \tag{9}$$

The pixel-to-intensity ratio is measured from the image of the gradient background, as discussed below in Fig. 4. The ratio of length with respect to pixels is measured from the experimental images and provides the physical distance relative to pixel size in the image plane. The length-to-pixels ratio is measured in the plane of the background and can represent the length-to-pixel ratio in any other plane if adjusted via trigonometry for the setup geometry.

The gradient images are created using MATLAB then displayed using a computer monitor as the background. This is similar to recent work using a computer monitor for a focusing schlieren source grid (Schoegl et al. 2016), but is the first time that a computer background has been used for BOS.

Images are recorded here with a Nikon D5100 camera. The images are recorded in color, then converted to grayscale via conversion to intensity (I) from the individual red (R), green (G), and blue (B) pixel values at each location:

$$I = \frac{1}{3}(R + G + B) \tag{10}$$

This method of conversion to a grayscale image is used over alternative methods to prevent biasing toward specific

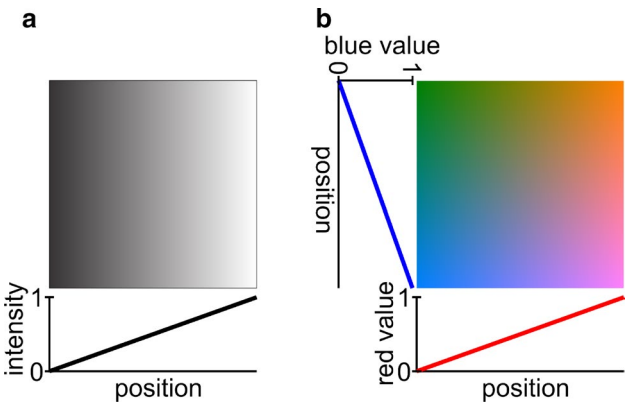

Fig. 3 **a** Grayscale gradient with horizontally varying values and **b** 2D gradient with varying *red* and *blue* values and constant *green* value of 0.5

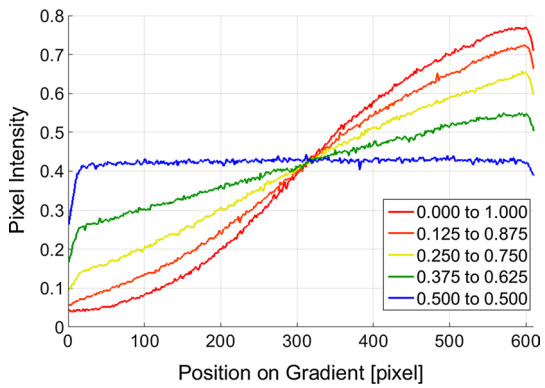

Fig. 4 Comparison of imaged grayscale intensities for displayed gradients with different minimum and maximum intensity variations. Decreases in intensity around locations of 0 and 600 px are associated with blurring at the edge of the gradient with the black surroundings on the monitor

colors (Gonzalez et al. 2009). The conversion is performed using a MATLAB script. This averaging also impacts the standard deviation in the intensity variations on the camera sensor. As discussed below, the standard deviation in pixel intensity in the green color plane was measured to be 0.0177, while the uncertainty in the grayscale measurements is about 0.004. Because the grayscale conversion averages the color planes together, the grayscale images have less sensor intensity noise.

The orientation of the gradient plays the same role as the orientation of a knife edge in traditional schlieren imaging (Settles 2001): refractions perpendicular to the gradient direction will not be imaged. This problem, however, can be avoided through the use of two-dimensional (2D) gradients. A two-dimensional color gradient background is created here by varying color intensities along individual axes of the image. In Fig. 3b a two-dimensional color gradient is created with red intensity varying along the *x*-axis and blue intensity varying along the *y*-axis of the image. The two-dimensional gradient background allows measurement of refractions in the *x*- and *y*-directions, or along any other direction in the shown two-dimensional plane. Analysis of the two-dimensional gradients is performed in RGB colorspace where the different colors can be independently extracted as two-dimensional matrices. The green plane of the image in Fig. 3b has a uniform 0.5 intensity. Other color gradient designs could be used for a particular purpose, as in color schlieren (Settles 2001), but the work here found that this simple linear variation was the most effective for simple quantitative measurements.

The background intensity variation must be measured from the recorded no-flow images because the camera will not necessarily reproduce color values from the computer-displayed image accurately. This was found to be especially apparent toward the edges of the gradients tested here. Inaccurate representation of the gradient can be a significant source of error if the background appearance is not examined directly. Figure 4 shows the measured intensity variation across gradients with different intensity value slopes. Each gradient was displayed at the same resolution and imaged from the same position with the Nikon D5100 camera.

The graph in Fig. 4 shows that even when the displayed gradient image ranges from pure black to pure white (0.000–1.000), the camera captures the minimum and maximum values as about 0.05 and 0.75, respectively, given the sensitivity, aperture, shutter settings, and lighting used. This gradient also has a nonlinear intensity variation in the recorded image, even though the displayed image had a perfect linear intensity variation. The gradients with smaller total variation resulted in a more linear gradient region.

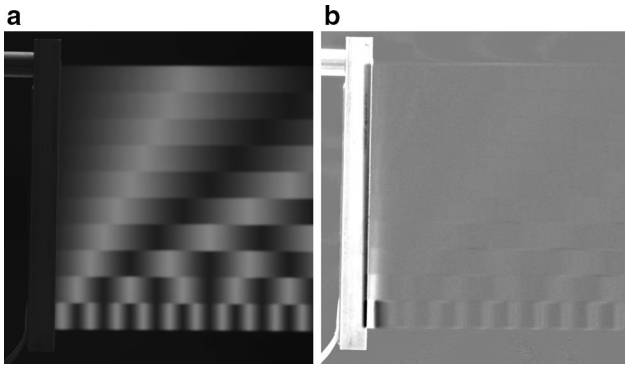

Fig. 5 **a** Raw image of a flat plate test with multiple gradient spacings in one background. **b** Processed gradient BOS image. Steeper gradients provide better BOS sensitivity but can be over-ranged, which requires more sophisticated processing

The inverse slope of a line in Fig. 4 is the pixel-to-intensity ratio that is required for Eq. 9.

Holding the size of a gradient constant and limiting the range of pixel values makes the BOS system less sensitive to small refractions; steeper gradients provide increased sensitivity because small refractions will cause a greater background intensity shift. To tune the sensitivity of the BOS system, gradients may be repeated in "stripes" to allow for a broader BOS analysis window. Repeating gradients can be effective for increasing system sensitivity, but can complicate the simplistic image subtraction analysis. Figure 5 shows a free-convection flat plate boundary layer test where regions of the background have differently sized gradient stripes to provide different BOS sensitivity. The steep gradients near the lower edge of the plate show a stronger response in the image subtraction (larger intensity variation), including the over-ranging of a single gradient. The over-ranging causes a reversal of the subtracted intensity values from near 1 to near 0. This over-ranging should be minimized, or a more sophisticated image subtracting algorithm implemented. The use of repeating stripes may also cause a decrease in the linear response region due to blurring of the edges of individual gradients; analysis of a composite gradient should be explored before testing to ensure the appropriate measurement range is attainable.

4 Experimental BOS setup considerations

Tests were performed with a Nikon D5100 DSLR camera with a 80- to 200-mm telephoto lens. Aperture settings ranged from *f*/2.8 to *f*/22 and were changed as appropriate for testing. Images were taken at the maximum resolution of the camera which is 3264 × 4928 pixels. The images were saved in 8-bit color depth by the camera. While much of the analysis was done in grayscale, all images were

taken in color and all image processing including conversion to grayscale was done in MATLAB.

All components of the gradient BOS system were arranged linearly through the use of optical rails and rail mounts. The computer monitor used as a background was on a multi-axis mount and aligned to be perpendicular to the camera at the desired position. The schlieren object and gradient background were aligned in the middle of the camera's field of view.

Once aligned, the background gradient was scaled to provide an adequately sized test region. This was done by adjusting the zoom of the gradient background image on the computer screen. All tests began with the object of interest in place, and flow images were taken before no-flow images. After flow images were taken, the object was simply removed to present a no-flow system. This was done where heating to steady state was required and to ensure the camera would not be physically touched during a test.

All efforts were taken to minimize movements of the system components during testing, because any movement could result in the creation of uncertainties larger than the pixel shifts to be measured. The camera was rigidly mounted and triggered with an IR remote, which allowed multiple images to be recorded. The Nikon camera automatic shutoff proved to be restrictive and required recording images every few seconds. A set of five images of the flow and background were averaged then used to obtain the data presented here. This was done to minimize camera sensor noise. The choice of five images was determined iteratively to be appropriate for analyzing the steady flow fields used here.

The least sensitive ISO setting of 100 was used which further reduced sensor noise. While noise was decreased, exposure time had to be increased to allow for sufficiently bright images. Shutter speeds here ranged from 1 s for an *f*/22 aperture to 1/20 s for an *f*/4 aperture. The limited light output of the computer screen limited the applications here to low-speed and laminar flow fields.

While ideal BOS imaging maintains a clear focus on both the schlieren object and background, this was not practical with the computer screen background. With a clear focus on the computer screen, an interference pattern was observed in recorded images due to imperfect alignment between the pixels of the screen and pixels of the camera sensor. To eliminate this, focus was maintained on the object of interest while the computer screen was left slightly out of focus. This is contrary to common BOS setup requirements (Hargather and Settles 2012), but the gradient background was not negatively affected by being out of focus except for areas close to the edges of the gradient. The interior of the gradient acts essentially in focus, even when slightly out of focus, and was found to be appropriate here for obtaining quantitative data.

Leaving the gradient background slightly out of focus allows the use of a relatively low-resolution monitor; a monitor with 1280 pixels × 1024 pixels and 48 cm diagonal length was used. The blurring of the out-of-focus background made individual pixels on the computer indiscernible and the gradient therefore was discretized by the resolution of the camera. Pixels were visible on speckle background tests where the computer monitor was in clear focus, but the pixel boundaries were relatively small compared to the speckle size and correlation window.

The *f*/4 aperture was the largest aperture capable of providing sufficient depth of field to capture both the object of interest and background in reasonable focus for *t*/*L* up to about 0.75. The *f*/22 aperture was appropriate for *t*/*L* ratios as low as 0.6. The variation in background appearance with aperture setting is shown in Fig. 6 for *f*/4 and *f*/22 with a *t*/*L* ratio of 0.6. As the background is more out of focus with the *f*/4 aperture, the background pixel values less resemble the linear trend that the background image was created to have. The edges of the gradient are also blurred with the surrounding color, resulting in changes in intensity slope

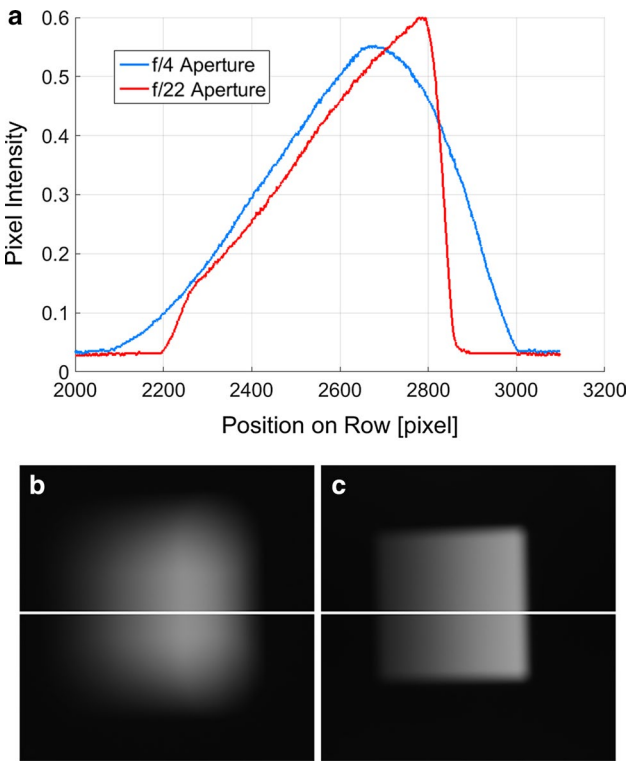

Fig. 6 **a** Comparison of intensity values across the gradient background along the highlighted row in images recorded with aperture settings of **b** *f*/4 and **c** *f*/22. The more in focus image (**c**) results in a more accurate reproduction of the linear background gradient. Quantitative data were measured only in the linear regions of the gradient and not near the edges of the gradient where blurring with the surrounding background occurs

near the boundaries, and the *f*/4 aperture resulted in a wider blurring of the boundary compared to the *f*/22 imaging.

Experiments were performed using a secondary light source to illuminate the computer screen in an attempt to reduce the exposure time for the images. Directing the illumination at the background screen resulted in glare on the background and test objects, which resulted in erroneous intensity shifts being measured. It was found that placing the light source behind the computer monitor increased the general room illumination and resulted in increased pixel intensities throughout the image. The increased intensities throughout the gradient resulted in a more linear gradient in dark regions while not overexposing light areas. The secondary light source allowed a decrease in shutter time by a factor of two (one stop). Increased ambient illumination also reduces effects of the monitor refresh rate, which can cause pixel intensity variation between individual images. Many modern digital cameras have autoexposure settings which can influence overall illumination appearance in the images. For all tests here, the camera was operated in manual mode and all settings remained the same and no changes were made to the white balance or autoexposure settings.

The system geometry was arranged to optimize data collected. Experiments were performed which varied the overall length of the system (L) and the ratio of camera-to-object length to camera-to-background length (t/L). For a fixed camera aperture, zoom, and background size, increasing the overall length of the system (L) and decreasing t/L both resulted in increased sensitivity, as shown in previous work (Hargather and Settles 2012). The increased sensitivity is observed in Figs. 7 and 8 as slope in the graphs of intensity variation between test and reference images increased. The increased slope represents increased sensitivity because the same points in the lens are producing a greater background intensity shift or pixel shift for the same refraction.

Ideally the BOS system will be as long as physically possible while still imaging the object and background with sufficient pixel resolution. The optimum value for t/L is not simply as small as possible though because of previously mentioned depth of field concerns. By increasing the sensitivity of the system through altering the physical placement of system components, desired trends can be better observed above the noise present. Figure 7 demonstrates that the noise on individual data lines is similar but the intensity change trend across the lens is more noticeable above the noise for the longer BOS system length L.

The camera aperture, camera lens focal length, camera pixel resolution, BOS system length L, and BOS system t/L ratio must all be balanced to provide the desired sensitivity for gradient BOS as in traditional BOS. The trade-offs for variations in each of these parameters are thoroughly discussed in previous literature (Hargather and Settles 2012; Bichal and Thurow 2010).

5 Experimental results

5.1 Grayscale analysis of calibration lens

Initial tests to assess the quantitative ability of gradient BOS were done with a calibration lens to provide a predictable and time-invariant refractive disturbance. Tests were performed to compare measured intensity shift to a predicted intensity shift based on the displayed gradient and system geometry. The displayed gradient had intensity values ranging from 0.25 to 0.75 and was sized to be just

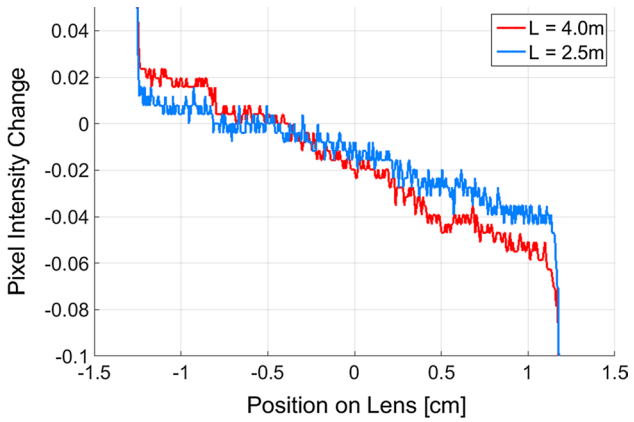

Fig. 7 Horizontal pixel intensity shift through middle of the 4 m focal length, 25.4-mm diameter lens for overall BOS system lengths L of 2.5 and 4.0 m. The increased slope for the longer overall system length indicates increased BOS sensitivity

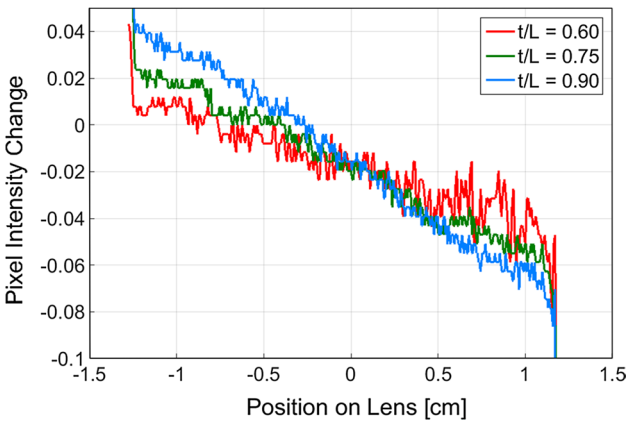

Fig. 8 Horizontal pixel intensity shift through middle of the 4 m focal length, 25.4-mm diameter lens for BOS systems with varied t/L ratios and a fixed overall length L of 4.0 m. The increased slope for the smaller t/L values indicate increased BOS sensitivity

larger than the diameter of the lens. The predicted intensity shifts were calculated using the angle of refraction through the lens at a given distance from the center of the lens, measured gradient intensity rate of change, and measured light transmittance of the lens (94 %).

The lens light transmittance was measured by finding the average of the ratio between intensity value near the location of the lens' center on a uniform green color plane with and without the lens in place. This was done with the green plane in images from the 2D BOS lens test seen in Fig. 12. The light transmittance values for the individual pixel locations in the region of interest near the center of the lens had a standard deviation of 0.0104. Only the center of the lens was used as light passing through the center is subject to minimal refraction.

Tests were performed with a distance between the camera and background of 4.0 m and a *t*/*L* ratio of 0.75. Five test images and five background images were averaged together to minimize camera sensor noise. The camera was set with a *f*/22 aperture and 1 second exposure.

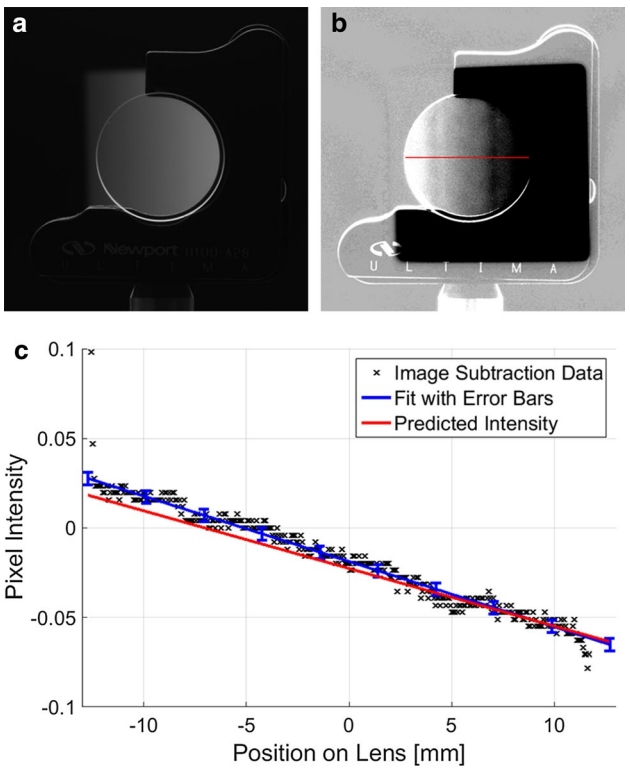

Fig. 9 **a** Test image of the lens in front of the gradient background (average of five individual images). **b** Gradient BOS image created through image subtraction, then histogram adjusted (for display purposes) to range of measured intensity change with medium gray as zero intensity shift. The row of pixels analyzed is highlighted in red across the middle of the lens. **c** Graph showing the measured and predicted intensity shift along the horizontal diameter of the lens

Figure 9 shows the BOS imaging and analysis of the calibration lens with the gradient background. There is a clear linear relationship between intensity shift and horizontal position on lens, as expected. The intensity shift should be zero at the center of the lens; however, it is shifted to one side due to the imperfect light transmission through the lens. Error bars on the fit line represent one standard deviation (0.0036) from the linear fit to the data points. The slope of the data fit line is comparable to the predicted slope to within the error bars.

Similar tests were performed with a gradient background covering only half of the lens width. In making the gradient vary between light and dark more rapidly, the shift signal was more noticeable in the image subtraction data, as shown in Fig. 10. Error bars on the fit line represent one standard deviation (0.0047) from the linear fit to the data points. The measured intensity variation

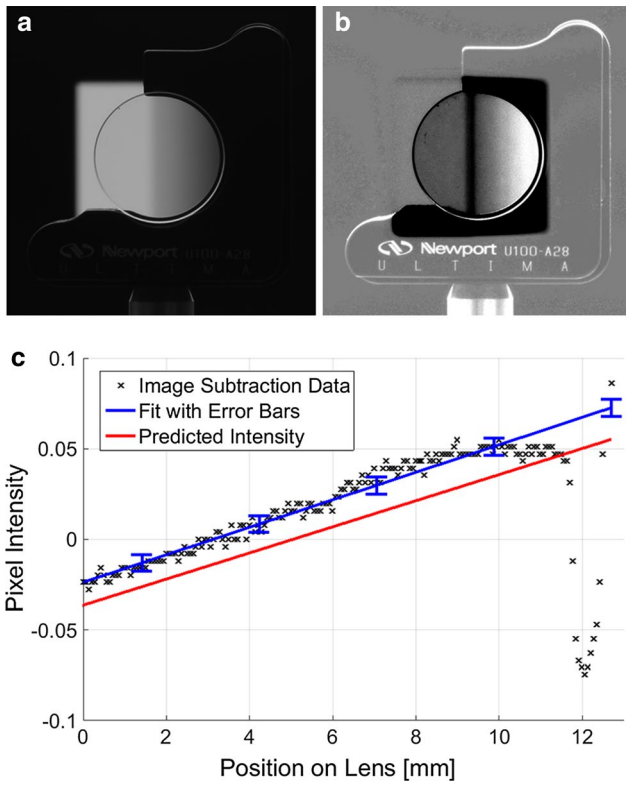

Fig. 10 **a** Test image of the lens in front of the gradient background (average of five individual images), with the gradient covering only half the lens. **b** Gradient BOS image created through image subtraction, then histogram adjusted (for display purposes) to range of measured intensity change with medium gray as zero intensity shift. The right edge of the vertical dark stripe through the lens is at the centerline of the lens, and all data to the left are not accurate because there is no gradient background behind that part of the lens. **c** Graph showing the measured and predicted intensity shift along the horizontal diameter of the lens. The large drop and rise in image subtraction data around 12 mm from the center of the lens is due to light being blocked by the lens mounting fixture

across the lens is closer to the predicted intensity variation. The vertical offset between the predicted and measured intensity variation is more prevalent in the half lens case because of higher-than-predicted apparent light transmission through the lens. The apparent transmission of light through the center of the lens in this case is 96 % which is due to the white region on the left side of the lens (used to aid in measuring lens location) acting as additional diffuse light source. This additional diffuse light increases intensity values throughout the surrounding image causing the increased apparent yet erroneous transmission. Ultimately the uncertainty in the transmission measurements here is approximately 3%, which overlays the prediction with the measured intensity profile. The slope of the intensity is more critical than the intercept, as the slope is used for the quantitative measurement.

5.2 Two-dimensional refraction measurements

The ability to measure two-dimensional refractions with gradient BOS is demonstrated with the calibration lens. The color gradient background used is shown in Fig. 11 in full color and as an intensity image of each color plane. The red and blue planes have horizontal and vertical gradients to measure horizontal and vertical refractions, respectively. The green plane is constant and can be used for baseline measurements like camera sensor noise and light transmission.

Images were recorded of the lens in front of the background with L of 4.0 m and t/L ratio of 0.75. Again, five images of the background and lens were each averaged to produce the data. The averaged image of the lens in front of the gradient is shown in Fig. 12a. Figure 12b–d shows the individual color planes of the image after background subtraction. Performing the image subtraction on individual color planes yields shifts in the direction of the gradient in the given color plane. The analysis within a single color plane provides the same information as a grayscale background varying linearly in one direction. In the case of the green color plane, no shift is observed as the plane is simply a uniform color field. The green plane could be constructed with another gradient direction if a particular shift is expected or of interest for a test, i.e., an angle across an oblique shock wave.

Results from a traditional BOS analysis with a speckle background are shown in Fig. 12e, f. The BOS analysis was performed using VIC-2D software by Correlated Solutions, Inc, with an interrogation window of 21 × 21 pixels and a step of 5 pixels. The background speckle pattern was displayed on the same computer monitor that the gradient images were displayed on. These images show the same linear image shift trends and data across the lens along coordinate axes as the color gradient BOS results.

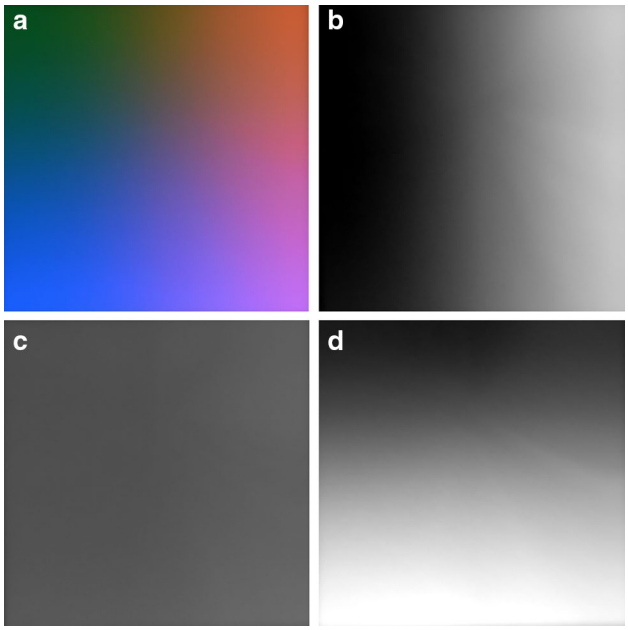

Fig. 11 Images of the color gradient background as **a** full color, **b** intensity image of *red* plane, **c** intensity image of *green* plane, and **d** intensity image of *blue* plane. The horizontal gradient in the *red* plane allows measurement of horizontal refractions, and the vertical gradient of the *blue* plane allows measurement of vertical refractions

To compare results from the two-dimensional gradient BOS analysis and traditional speckle background BOS, refraction angles were calculated and compared to theory through multiple diameters through the lens. The diameters were along lines of 0°, 45°, and 90° from horizontal. Refraction angles were calculated from measured shifts in the x- and y-directions (vertical and horizontal, respectively, in the image) and setup geometry. The measured refraction angles agree well with theory for both gradient and traditional methods. The data to the left of −2 mrad on the 90° and 0° directions in (a) and (b), respectively, diverge from the theory because these points are in a nonlinear region of the gradient background. The vertical trends of the 0° diameter on the ε_x plot and the 90° diameter on the ε_y plot occur due to camera sensor noise and can be taken as a maximum bound to the uncertainty in the measurements taken. The grayscale data presented in Fig. 13b are the same as presented in Fig. 9 but converted to refraction angle from intensity change. The graphs show there is no significant variation in uncertainty between the color planes, directions through the lens, or compared to using a grayscale background.

With the two independent shift directions imaged in the red and blue color planes, two-dimensional refraction can be quantified. Visualization of the two-dimensional refractions is done by converting the image shifts in the red and blue planes along Cartesian axes to a polar space defined

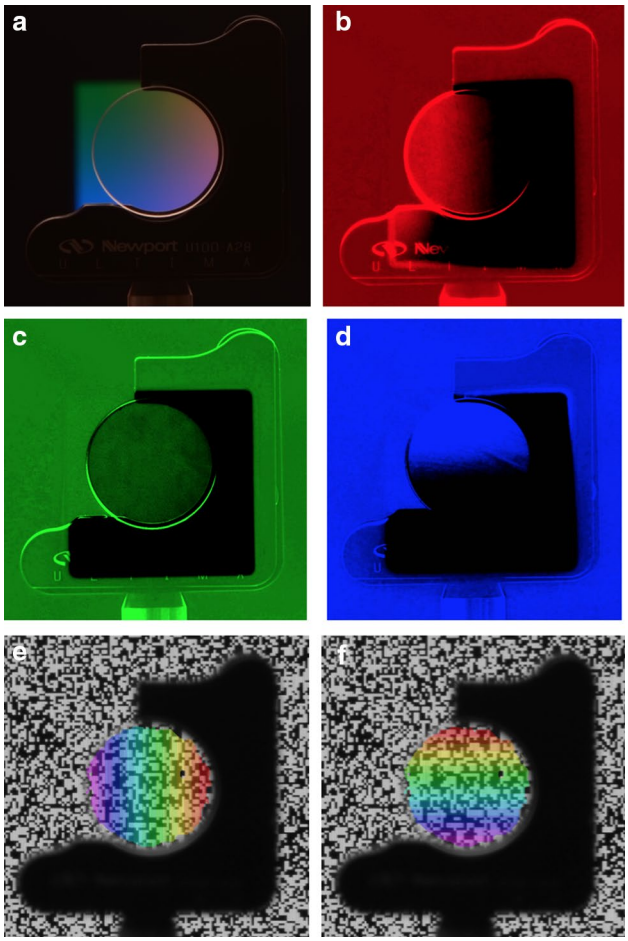

Fig. 12 **a** Averaged image of the calibration lens in front of the color gradient background in full color. The background image is subtracted from (**a**) to yield the BOS result, which is shown here in individual color planes: **b** *red*, **c** *green*, and **d** *blue*. Traditional BOS analysis with a speckle background reveal the same data for **e** horizontal and **f** vertical pixel shifts

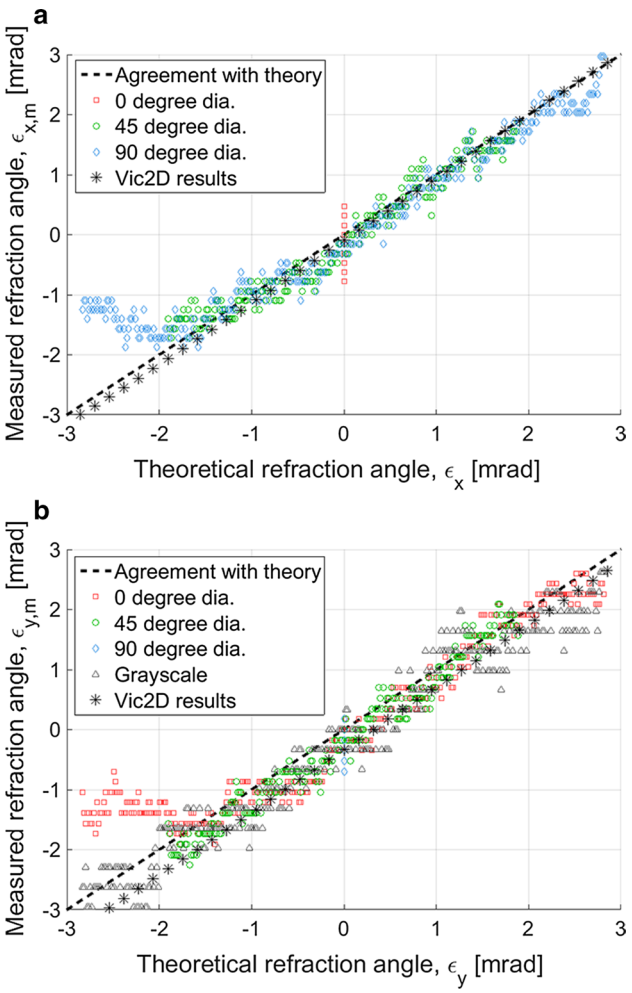

Fig. 13 Measured two-dimensional gradient BOS and traditional speckle BOS ($\varepsilon_{x,m}$ and $\varepsilon_{y,m}$) compared to theory (ε_x and ε_y) for calibration lens. Refraction angles are calculated in terms of vertical (**a**) and horizontal (**b**) components. Perfect correlation between experimental data and theory occurs along a *line* through the origin with a slope of one

by magnitude and direction of the shift. Matrices describing the magnitude and direction of the overall shift are calculated in MATLAB and are then used as planes in a HSV (hue, saturation, value) color model. Hue is used to map the angle of the shift between 0° and 360°, where red represents 0°, green is 120°, and blue is 240°. The saturation plane is used to show the magnitude of the color shift, where zero shift is unsaturated and the maximum shift observed in the tests is scaled to a saturation value of 1. This yields locations of no shift appearing white and locations of maximum shift being saturated at full color. The value plane is held constant in this representation. With this visualization approach, the multi-directional refractive disturbances are all completely represented by the color in the image. Figure 14 shows a traditional vector plot with

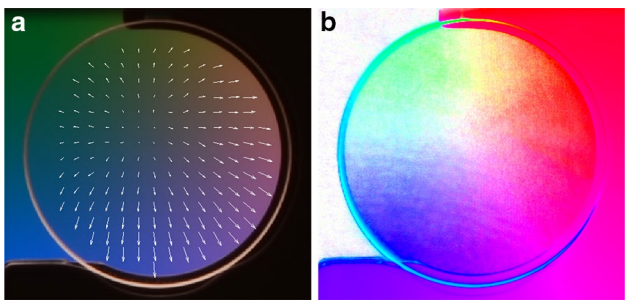

Fig. 14 Two-dimensional gradient BOS refraction measurements as **a** vector plot on original image and **b** HSV image with the hue plane representing the direction of the shift and the saturation plane representing the magnitude of the refraction

the vectors showing the direction and magnitude of the pixel shifts and the developed HSV display approach. It can be seen that the smallest shifts through the lens occur toward the center, reaching zero at a point, and the large shifts toward the outer edges occur radially outwards from the center. The apparent zero shift location is slightly off-center in the image due to the less than 100 % light transmission of the lens.

5.3 Laminar free-convection flat plate boundary layer

The flat plate was aligned with the centerline of the field of view and then heated until a steady-state surface temperature of 333.9 K was observed. This provided a 36.0 K difference from the ambient room temperature of 297.9 K. The overall distance (L) between the camera and LCD monitor background was 4.0 m, and the t/L ratio was 0.75. The extent of the flow field (Z) is assumed the same as the width of the plate, measured as 152 mm, and the flow is considered uniform over the plate width. When the plate reached steady state, flow images were recorded with the plate in place and then the plate was removed to record the no-flow background images. An aperture of $f/16$ for gradient background images and $f/22$ for the speckle background images was used with a 0.5-s exposure. Test and background images were converted to grayscale and then averaged over five images to minimize random noise from the camera sensor. Averaging of the test images did not affect the flow images because the convection from the plate was laminar and steady. The final averaged background and flow images are shown in Fig. 15 along with the processed gradient BOS image.

The gradient BOS image produced from the image subtraction shows the intensity shifts associated with the convection from the plate. The gradient BOS image has been histogram-stretched to enhance the visibility of the refractive shifts. The BOS results are histogram-adjusted to show zero shift regions as medium gray and scaled to show shifts between ± 0.05 in the original image on the range of 0 to 1. The histogram stretching is done for visualizing the flow field, but all quantitative refractive gradient calculations are done on the un-adjusted image. The horizontal background gradient only reveals the horizontal refractions, so the two-dimensional flow at the flat plate leading edge is not fully resolved.

Analysis of the density field was performed along the highlighted line in Fig. 15c, a distance of 76 mm from the leading edge of the plate. The resulting BOS visualization is qualitatively similar to traditional BOS and schlieren imaging of the same flow field performed by Hargather and Settles (2012).

To further reduce the pixel-to-pixel intensity noise from the camera, the row of pixels being analyzed was averaged with the three rows above and below it. From the pixel resolution, this is equivalent to analyzing a vertical space of 0.48 mm as a single point. The pixel intensity profile along the line in Fig. 15c is shown in Fig. 16. A clear trend between intensity shift and distance away from the surface of the plate is observed. Without proper focus, the data points closest to the flat plate surface have increased variability due to blurring of the image at the edge of the plate.

Relating the image subtraction data to the rate at which intensity of the background varies horizontally yields the pixel shift at each location using Eq. 9. Equation 2 is then

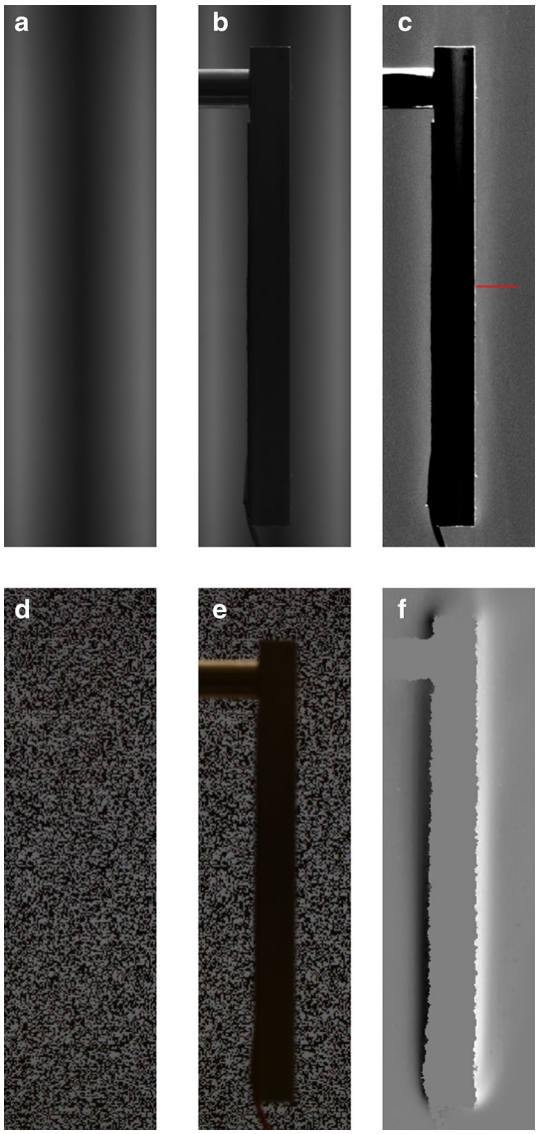

Fig. 15 Averaged **a** background image and **b** flow image are subtracted to yield the **c** gradient BOS image, while image correlation is performed on the speckle background images no-flow (**d**) and flow (**f**) to get an image representing horizontal shift values (**e**). The highlighted *red line* in (**c**) is the location where data are being analyzed

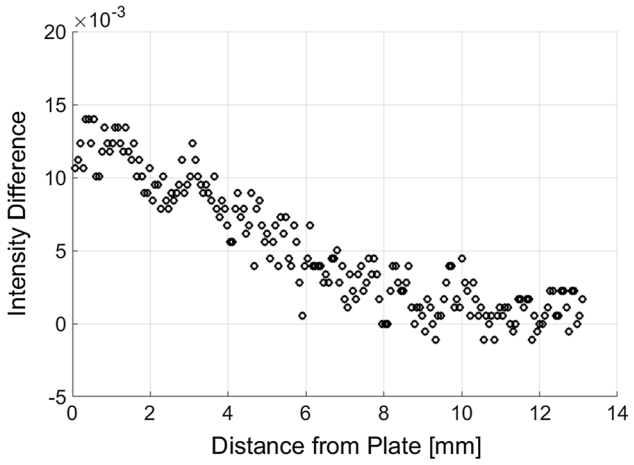

Fig. 16 Intensity variation in gradient BOS image as a function of distance from the plate surface along the line in Fig. 15c

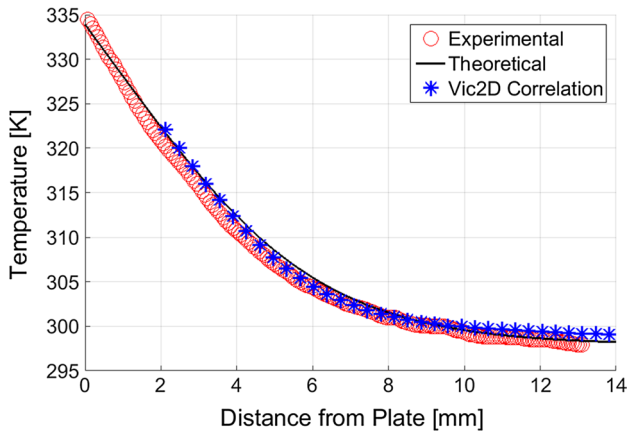

Fig. 17 Measured temperature as a function of distance from the flat plate surface for gradient BOS and traditional speckle BOS compared to the theoretical temperature distribution along the highlighted line in Fig. 15c

used to obtain the refraction angle at each location from the plate surface. The index of refraction gradient field is calculated from Eq. 3, then integrated to give the index of refraction at each location. The density field is finally calculated from the local index of refraction using the Gladstone-Dale Law (Eq. 4). The temperature field is obtained from the density field assuming that the pressure throughout the boundary layer is ambient pressure. The measured temperature field is shown in Fig. 17 along with the theoretical distribution calculated from Ostrach's work (1952). The measured and theoretical temperature fields agree well, and the size of the experimental data symbols in Fig. 17 represent the estimated error in the calculation of the temperature. Gradient BOS analysis calculates a plate surface temperature of 334.5 K compared to the directly measured surface temperature of 333.9 K.

Additional images were taken of the same flat plate test with a traditional speckled background and camera focus adjusted to the background plane. Traditional image correlation-based BOS analysis was done with the flow and no-flow images with the speckled background. The images with traditional BOS backgrounds were processed using the VIC-2D software with a window size of 21 × 21 pixels and step of 5 pixels. The horizontal shift information was then used to calculate a temperature profile in the same manner as the gradient BOS analysis. This temperature profile can be seen in Fig. 17. Both temperature profiles calculated from traditional and gradient BOS were able to provide similar trends to theory. Traditional correlation was not able to be performed closer than 2 mm from the surface of the flat plate because of significant blurring of the image due to focus needing to be on the background. However, the ability to focus on the object of interest in the gradient BOS test allows for accurate temperature data to be collected to the surface of the plate with sharp focus.

5.4 Uncertainty evaluation

The gradient BOS measurement uncertainty can be estimated from the green plane of the averaged images presented in Fig. 11a since the background in this color plane should be a uniform color. The average pixel intensity in the green background image is 0.3298 with a standard deviation of 0.0177. Using Eqs. 2 and 9, the calculated standard deviation and average intensity values correlate to a refraction angle uncertainty at a single pixel location of 0.41 mrad. This uncertainty is comparable to the random scatter about the theoretical line in Fig. 13. Uncertainty associated with geometry and atmospheric conditions is found to be relatively insignificant compared to the intensity variations.

For calculating the uncertainty in the temperature measurement, multiple refraction measurement are incorporated as part of the integral process. Using multiple individual intensity measurements, each with its own individual random error, allows the use of an average uncertainty for the intensity variation (Figliola and Beasley 2010). The average uncertainty is calculated from the individual uncertainty (σ) and the number of samples (N):

$$\bar{\sigma} = \frac{\sigma}{\sqrt{N}} \tag{11}$$

From the sample size of 77,442 pixels in the square background region in Fig. 11, the resulting average uncertainty in the refraction angle is 1.5 μrad. From this, an approximation can be made on the uncertainty in the flat plate surface temperature calculated from gradient BOS analysis. This is done with calculated parameters based off the measured angle of refraction of −0.727 mrad at the surface of the

plate, then propagating the error through Eqs. 3, 4, and the ideal gas law. The resulting uncertainty in the calculated plate surface temperature is ±0.68 K. The directly measured surface temperature of the plate (333.9 K) is within the range of the calculated surface temperature (334.5 K) when considering this measurement uncertainty.

The effects of chromatic aberration were not considered here. These effects could be important, dependent on setup, lens, and background color choice, but likely are insignificant if high-quality lenses are used.

6 Conclusions

Gradient backgrounds were used successfully for quantitative BOS analysis of a calibration lens and a laminar free-convection flat plate boundary layer. Initial testing yielded observations for tuning multiple characteristics of the gradient BOS system for higher-quality quantitative data, including suggestions for the system geometry, gradient selection, and camera settings. One-dimensional grayscale testing with a 4-m-focal-length lens provided pixel intensity shift data which compared well with theoretical expectations of light refraction. Flat plate testing yielded quantitative temperature field measurements through the laminar boundary layer calculated from measured intensity shifts and the ambient room temperature, which also compared well to theory. The BOS images created from the gradient background provide comparable visualizations to traditional BOS and schlieren images presented in the literature.

A two-dimensional BOS analysis was introduced using a background image with gradients along individual directions in separate color planes of a RGB color image. Image shifts were quantified for the calibration lens along two independent axes which were used to calculate overall direction and magnitude of the shifts. This was then displayed systematically in a single color image using a hue-saturation-value (HSV) color representation.

Additionally, the successful use of an LCD screen as a means to display digitally created backgrounds on demand was demonstrated.

Limitations to the implementation of gradient backgrounds in BOS include camera sensor noise, improper representation of color by the camera, and irregular or inconsistent backgrounds. Camera sensor noise becomes an issue as the color shifts in gradient BOS are rather small and can sometimes be masked by noise in pixel color values which is a result of the capabilities of the digital camera in use. If the camera does not accurately represent the colors or color trends in an image, there is the possibility for error in post-processing calculations. If a background gradient is not linear, then calculations to determine the magnitude of pixel shifts become more difficult. Here, a linear gradient was used for simplicity. A more sophisticated analysis could be performed with a nonlinear background variation, if the appropriate care is taken and the background pattern can be clearly distinguished above the sensor noise. While BOS analysis of steady-state events have been shown here, the basic concepts of implementing a color gradient as a background would remain the same for time-varying flows. Gradient sizing and lighting would be major factors in testing of time-variant systems, especially if a LCD monitor was used as the background. The applications of this gradient BOS technique could be effectively implemented in low-light scenarios by using traditional printed backgrounds which could be sufficiently illuminated.

References

Atcheson B, Heidrich W, Ihrke I (2009) An evaluation of optical flow algorithms for background oriented schlieren imaging. Exp Fluids 46(3):467–476. doi:10.1007/s00348-008-0572-7

Bauknecht A, Ewers B, Wolf C, Leopold F, Yin J, Raffel M (2015) Three-dimensional reconstruction of helicopter blade-tip vortices using a multi-camera BOS system. Exp Fluids 56(1866):1–13. doi:10.1007/s00348-014-1866-6

Bichal A, Thurow B (2010) Development of a background oriented schlieren based wavefront sensor for aero-optics. In: 40th AIAA fluid dynamics conference, AIAA 2010-4842

Dalziel S, Hughes G, Sutherland B (2000) Whole-field density measurements by 'synthetic schlieren'. Exp Fluids 28(4):322–335. doi:10.1007/s003480050391

Elsinga GE, Oudheusden BWV, Scarano F, Watt DW (2004) Assessment and application of quantitative schlieren methods: calibrated color schlieren and background oriented schlieren. Exp Fluids 36(2):309–325

Figliola RS, Beasley DE (2010) Theory and design for mechanical measurements. Wiley, New York

Gonzalez RG, Woods RE, Eddins SL (2009) Digital image processing using MATLAB. Gatesmark Publishing, New York

Hargather MJ (2013) Background-oriented schlieren diagnostics for large-scale explosive testing. Shock Waves 23:529–536. doi:10.1007/s00193-013-0446-7

Hargather MJ, Settles GS (2010) Natural-background-oriented schlieren. Exp Fluids 48(1):59–68

Hargather MJ, Settles GS (2012) A comparison of three quantitative schlieren techniques. Opt Lasers Eng 50:8–17

Kumar R, Ali MY, Alvi FS, Venkatakrishnan L (2011) Generation and control of oblique shocks using microjets. AIAA J 49(12):2751–2759. doi:10.2514/1.J051148

Leopold F (2009) The application of the colored background oriented schlieren technique (CBOS) to wind tunnel, free-flight and in-flight measurements. J Flow Vis Image Process 16(4):279–293. doi:10.1615/JFlowVisImageProc.v16.i4.10

Ostrach S (1952) An analysis of laminar free-convection flow and heat transfer about a flat plate parallel to the direction of the generating body force. Technical report 2635, NACA

Ota M, Leopold F, Noda R, Maeno K (2015) Improvement in spatial resolution of background-oriented schlieren technique by introducing a telecentric optical system and its application to supersonic flow. Exp Fluids 56(48):1–10. doi:10.1007/s00348-015-1919-5

Raffel M (2015) Background-oriented schlieren (BOS) techniques. Exp Fluids 56(60):1–17. doi:10.1007/s00348-015-1927-5

Raffel M, Richard H, Meier GEA (2000) On the applicability of background oriented optical tomography for large scale aerodynamic investigations. Exp Fluids 28(5):477–481

Richard H, Raffel M (2001) Principle and applications of the background oriented schlieren (BOS) method. Meas Sci Technol 12(9):1576–1585

Schoegl I, Pisano AJ, Sedky G (2016) Development of a compact focusing color schlieren technique. In: 54th AIAA aerospace sciences meeting, San Diego, CA, USA, AIAA 2016-1765

Settles GS (2001) Schlieren and shadowgraph techniques: visualizing phenomena in transparent media. Springer, Berlin

Tan DJ, Edgington-Mitchell D, Honnery D (2015) Measurement of density in axisymmetric jets using a novel background-oriented schlieren (BOS) technique. Exp Fluids 56(204):1–11. doi:10.1007/s00348-015-2076-6

Venkatakrishnan L, Meier GEA (2004) Density measurements using the background oriented schlieren technique. Exp Fluids 37(2):237–247

Venkatakrishnan L, Suriyanarayanan P (2009) Density field of supersonic separated flow past an afterbody nozzle using tomographic reconstruction of BOS data. Exp Fluids 47(3):463–473. doi:10.1007/s00348-009-0676-8

Venkatakrishnan L, Suriyanarayanan P, Jagadeesh G (2013) Density field visualization of a micro-explosion using background oriented schlieren. J Vis 16(3):177–180